Supplementary Information

Design of Zn-MOF the Biosensor via a Ligand "Lock" for the Recognition and Distinction of S-containing Amino Acids

Xiao-Qin Wu,[a,b] Yan Liu, [b] Pei-Qi Feng,[a] Xue-Hong Wei,[a] Xiao-Hang Qiu [b]* and Jian-Gong Ma,[b]*

Experimental Part

1.1 Chemicals and Instrumentation

Zinc(II) nitrate ($Zn(NO_3)_2·6H_2O$, 99%), 2,5-thiophenedicarboxylic acid (H_2L, >95%), 2,2'-dipyridyl (bipy, >99%) N,N-dimethylacetamide (DMA, >99%), *L*-cysteine (*L*-Cys, >99%), *L*-methionine (*L* -Met, >99%) and *L* -cystine (*L* -Cys-Cys, >99%) were purchased from commercial suppliers (Aladdin-reagent and J&K-reagent) and were used as received without further purification. All solutions were prepared with ultrapure water.

The phases were analyzed by X-ray powder diffraction (XRD) using a D/Max-2500 X-ray diffractometer with Cu Kα radiation. The FT-IR spectra were measured with a Bruker Tensor 27 spectrophotometer on KBr disks. TGA experiments were performed on a NETZSCH TG 209 instrument with a heating rate of 10 ℃ min^{-1}.

The crystal data were collected by an Agilent Technologies SuperNova Single Crystal Diffractometer. The phases were analyzed by X-ray powder diffraction (XRD) using a D/Max-2500 X-ray diffractometer with Cu Kα radiation. The FT-IR spectra were measured with a Bruker Tensor 27 spectrophotometer on KBr disks. TGA experiments were performed on a NETZSCH TG 209 instrument with a heating rate of 10 ℃ min^{-1}.

1.2 Synthesis of $\{[Zn_2(L)_2(\mu_2\text{-}O)(H_2O)_3]·2DMA\}_n$ (Zn-1)

A mixture of 59.50 mg (0.2 mmol) $Zn(NO_3)_2·6H_2O$ and 46.04 mg (0.2 mmol) H_2L was dissolved in a mixture of 5 mL DMF and 5 mL H_2O, and then heated for 2 days at 90 ℃ in a Parr Teflon-lined stainless steel vessel (23 mL), then cooled to room temperature slowly in 2 days. Colorless sheet crystals of **Zn-1** were collected at the bottom of the glass vessel. Yield: 44.2 mg (81.7 %). Anal. Calc for $C_{12}H_{10}O_{12}S_2Zn_2$: C, 26.2; H, 1.8; Found: C, 25.8; H, 2.0; IR: 3078.49 w, 1589.16 m, 1557.10 s, 1529.78 s, 1516.84 m, 1493.22 w, 1465.58 w, 1429.83 m, 1361.03 s, 1337.20 s, 1316.06 m, 1220.59 w, 1140.48 m, 1103.23 m, 1049.37 w, 1023.70 w, 867.15 s, 845.51 s, 809.90 s, 784.79 m, 770.77 s. 723.13 s, 684.60 w.

1.3 Synthesis of $\{[Zn_2(L)_2(2,2'\text{-bipy})(\mu_2\text{-}O)(H_2O)_2]_n\}$ (Zn-2) from Zn-1

We chose several single crystals of **Zn-1** which was synthesized followed by the steps based on the above description of **1.2**, and then these **Zn-1** single crystals were put in a glass bottle with 0.03 mM auxiliary ligand 2,2'-dipyridyl (solvent: mixture of DMF and H_2O 2:1,v/v). It heated for 2 days at 90 ℃, then cooled to room temperature slowly in 2 days. Colorless diamond-like crystals of **Zn-2** were converted form **Zn-1** can be collected at the bottom of glass bottle. The phase purity of **Zn-1** and **Zn-2** were confirmed by the PXRD methods (See Fig. S3 and S4).

1.4 Synthesis of {$[Zn_2(L)_2(2,2'\text{-bipy})(\mu_2\text{-}O)(H_2O)_2]_n$} (Zn-2) directly

A mixture of 59.50 mg (0.2 mmol) $Zn(NO_3)_2 \cdot 6H_2O$, 31.24 mg (0.2 mmol) 2,2'-dipyridyl and 46.04 mg (0.2 mmol) H_2L was dissolved in a mixture of 5 mL DMF and 5 mL H_2O, and then heated for 2 days at 90 ℃ in a Parr Teflon-lined stainless steel vessel (23 mL), then cooled to room temperature slowly in 2 days. Colorless diamond-like crystals of **Zn-2** were collected at the bottom of the vessel. Yield: 45.4 mg (86.9 %). Anal.Calc for $C_{22}H_{15}N_2O_{11}S_2Zn_2$: C, 38.96; H, 2.23, N, 4.12; Found: C, 38.92; H, 2.30, N, 4.10 (%); IR: 3201.41 w, 1606.01 s, 1586.54 s, 1572.69 m, 1528.66 w, 1472.53 s, 1489.04 w, 1439.22 s, 1351.31 s, 1311.23 s, 1248.74 m, 1211.33 m, 1169.12 w, 1152.21 m, 1108.20 w, 1055.50 w, 1040.77 m, 1023.93 m, 823.41 m, 795.16 s, 771.75 s, 760.80 s, 736.93 s, 684.16 m, 651.29 m.

2. Characterization

2.1 X-ray crystallography

Diffraction intensity data for single crystals of **Zn-1** and **Zn-2** were collected on a Agilent Technologies SuperNova Single Crystal Diffractometer at 293 (2) K equipped with graphite-monochromatic Mo Kα radiation (λ = 0.71073 Å). The structures were solved by SHELXS (direct methods) and refined by SHELXL (full matrix least-squares techniques)[1] in the Olex2 package.[2]

Table 1. Crystal data and structure refinements for **Zn-1** and **Zn-2**

	Zn-1	**Zn-2**
formula	$C_{12}H_{10}O_{12}S_2Zn_2$	$C_{22}H_{15}N_2O_{11}S_2Zn_2$
M, g mol^{-1}	522.35	678.22
crystsyst	Monoclinic system	Triclinic system
space group	*P*2/m	*P*-1
a / Å	14.4432(3)	11.1191(10)
b / Å	15.7741(3)	11.1367(10)
c / Å	15.7204(4)	15.4541(14)
α / deg	90.00	87.029(3)
β / deg	104.090(3)	86.265(3)
γ / deg	90.00	84.741(3)
V / Å^3	3448.6(7)	1899.6(3)
Z	2	2
reflns collected	6308	6624
unique reflns	4839	6200
R1 [I > 2σ(I)]	0.1236	0.0874
wR2(all data)	0.3601	0.2310

1. G. M. Sheldrick,*ActaCryst.*, 2008, **A64**, 112-122
2. O. V. Dolomanov, L. J. Bourhis, R. J. Gildea, J. A. K. Howard and H. Puschmann, *J. Appl. Cryst.*, 2009, **42**, 339-341.

1.4 Thermal Gravimetric Analyses.

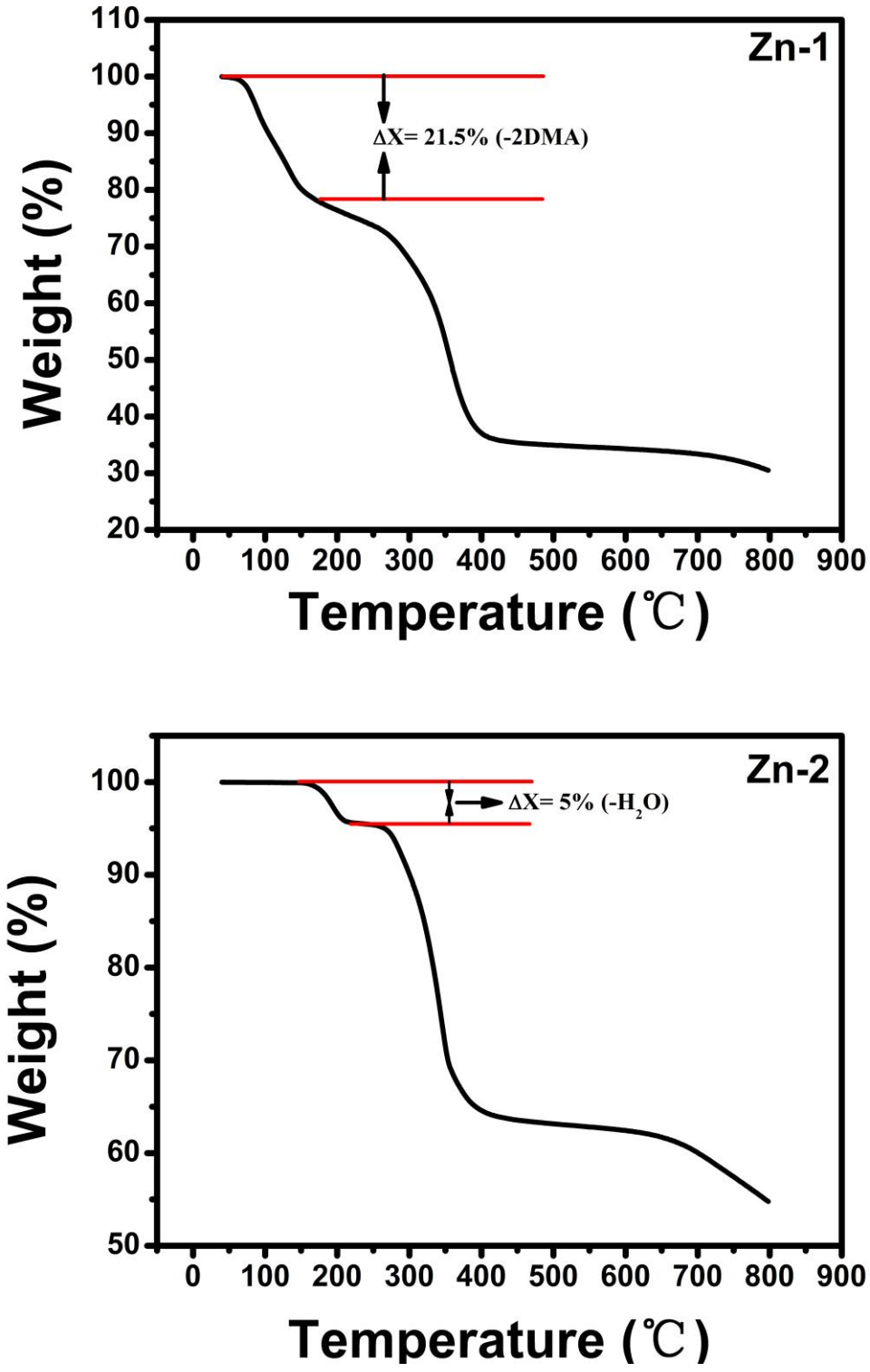

Fig. S1. Thermal gravimetric analyses (TGA) of **Zn-1** and **Zn-2**

1.5 Powder X-ray Diffraction patterns

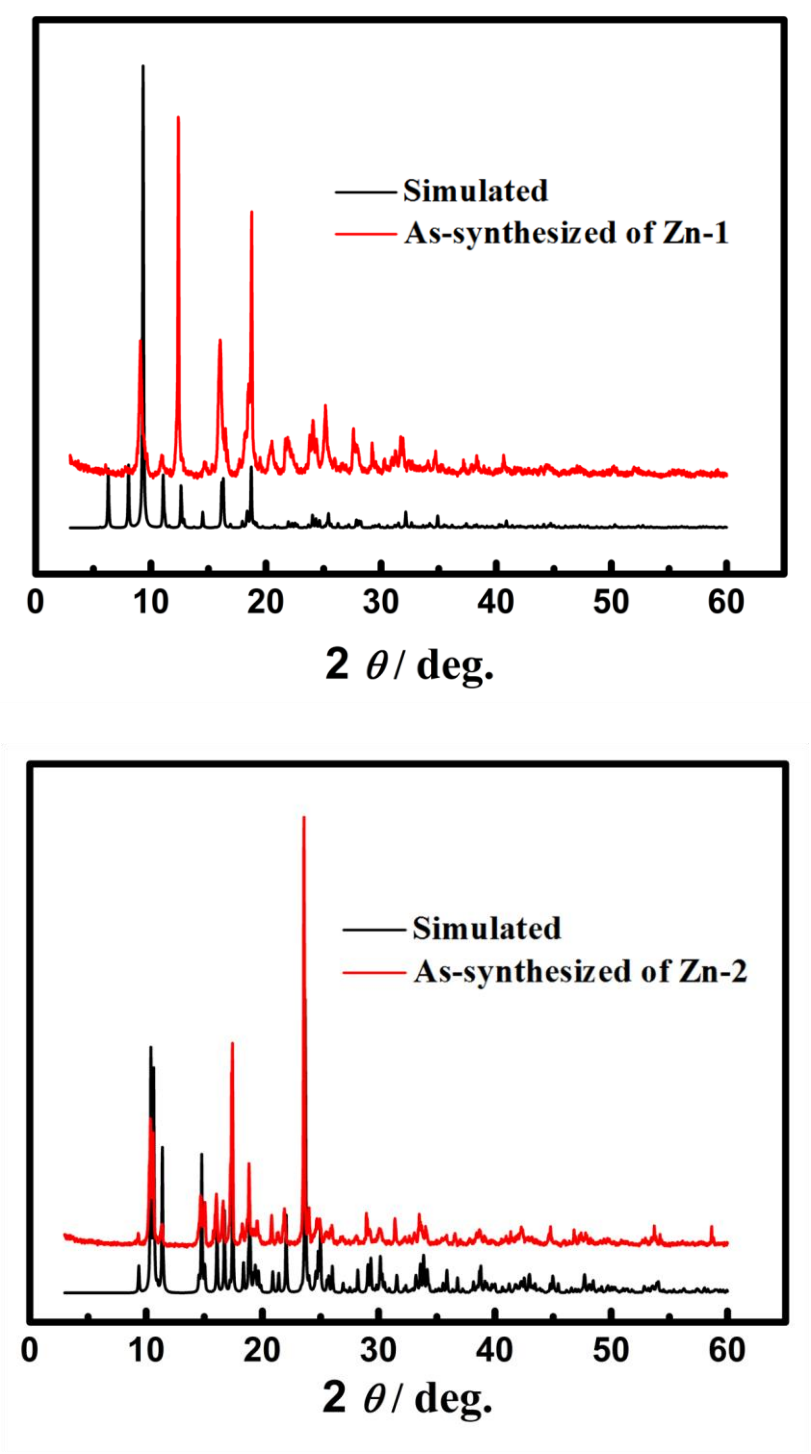

Fig. S2. PXRD patterns of the simulated one from single-crystal date of **Zn-1** and **Zn-2,** compare with the samples **Zn-1** and **Zn-2** as synthesized, respectively.

Fig. S3. Single crystal conversion of **Zn-1** to **Zn-2**

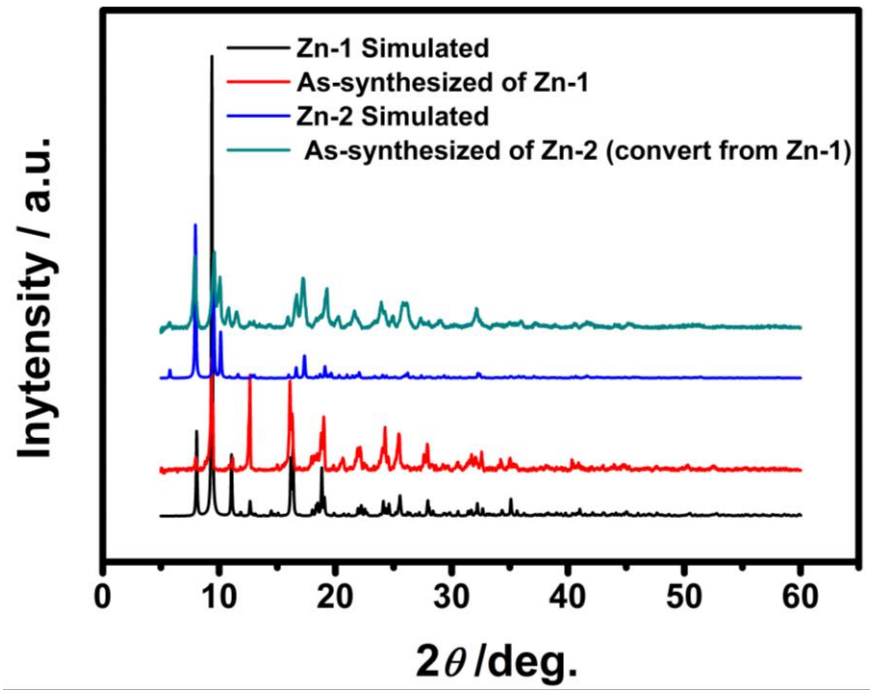

Fig. S4. PXRD patterns of the simulated one from single-crystal date of **Zn-1** and **Zn-2,** compare with the samples **Zn-1** as synthesized and **Zn-2** convert from **Zn-1**, respectively.

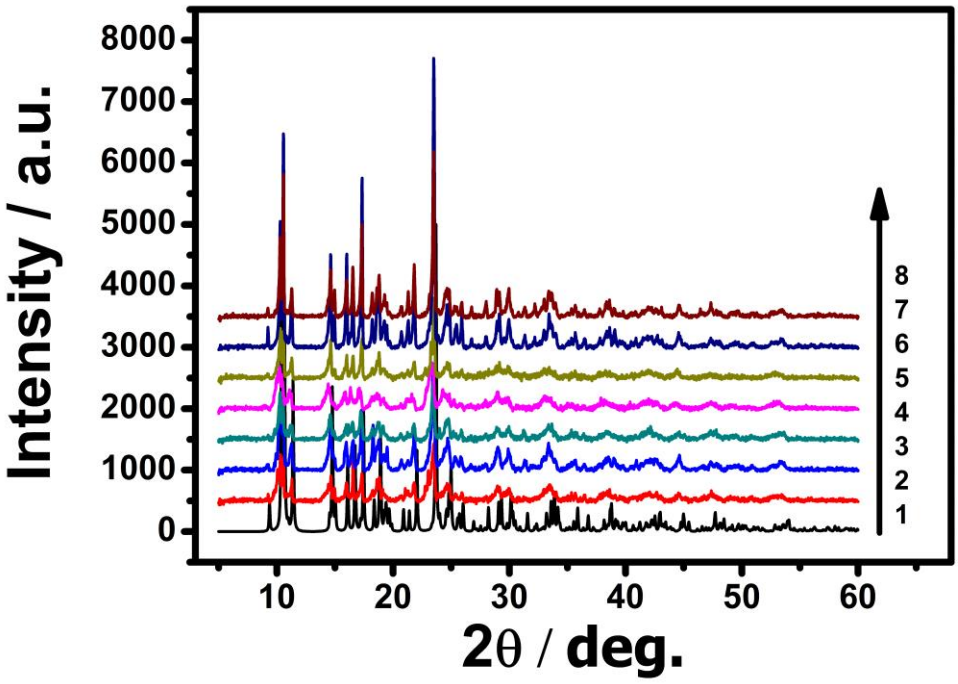

Fig. S5. PXRD patterns of the simulated one from single-crystal date of **Zn-2** (1) compare with PXRD the patterns for **Zn-2** after immerse in ethanol (2), DMF (3), DMA (4), acetonitrile (5), Methanol (6), tetrahydrofuran (7), dichloromethane (8) for two weeks, respectively.

3. Electrochemical Section

Cyclic Voltammetry (CV) Analysis: A Chi660e electrochemical workstation (China) was used for CV studies.

Three-electrode system was used as follow:

Working electrode (WE): **Zn-2** coated on an Au electrode (**AuE**), named **Zn-2/AuE,** was used as working electrodes.

Reference electrode (RE): 0.1M AgNO3-acetonitrile solution as electrode solution was filled into a silver ion electrode (SIE).

Auxiliary electrode (AE): a platinum wire electrode was used as the auxiliary electrode in the whole work.

Electrolyte: 0.5 mol/L [Bmim]BF_4 in DMF solution (DMF-$BMIMBF_4$).

All studies were carried out at room temperature and under nitrogen surroundings.

Prior to be used, the bare AuE was carefully polished with an alumina slurry (0.5 μm particle size) until a mirror-like surface was obtained, then rinsed ultrasonically with ultrapure water, nitric acid (1:1, v/v), sodium hydroxide (0.1 $mol \cdot cm^{-3}$) and ethanol, respectively, to remove any alumina residue from the electrode surface. The ultrasonicate process was handled with an ultrasonic cleaning machine (Elma, S100H).

Electrode modification was performed as follow: depositing 0.025g **Zn-2** dissolved in the nafion solution and 10 μL of this solution were putting on the AuE surface. Then a clean beaker was coated

on the modified electrode, which dried in the air for 12 h.

Impedance Analysis: Electrochemical Impedance Spectroscopy (EIS) was performed using a Chi660E electrochemical workstation (China). All samples were collected using the above three-electrode system in 10 mL DMF-$BMIMBF_4$ solution, which act as an electrolyte, EIS frequency was cycled between 0.1 Hz –100 kHz.

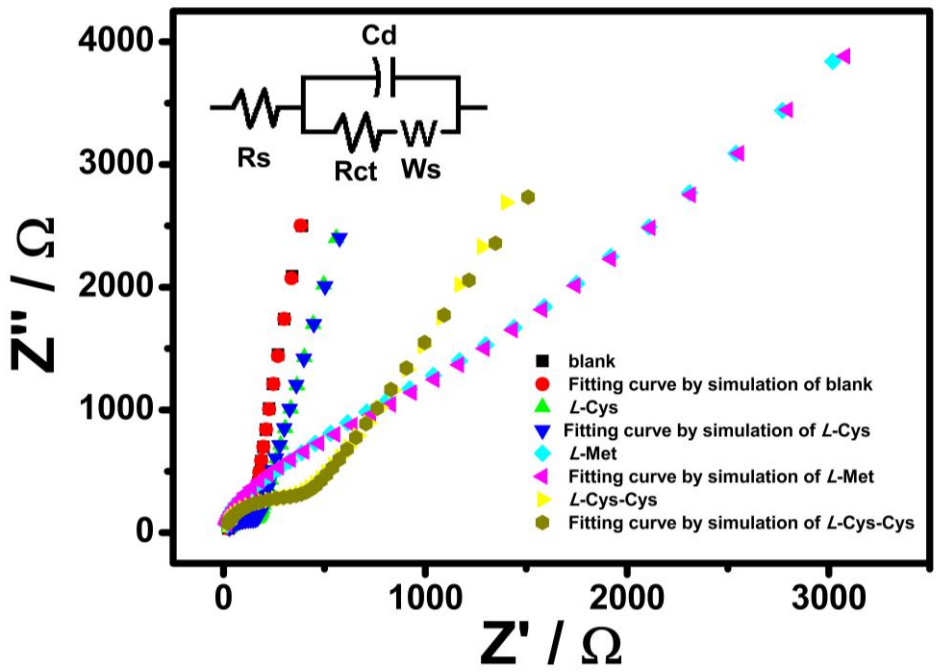

Fig. S6. Nyquist plots and fitting curves of Zn-2/AuE in DMF-BMIMBF4 solution or containing 0.5 mM L-Cys, L-Met and L-Cys-Cys, respectively

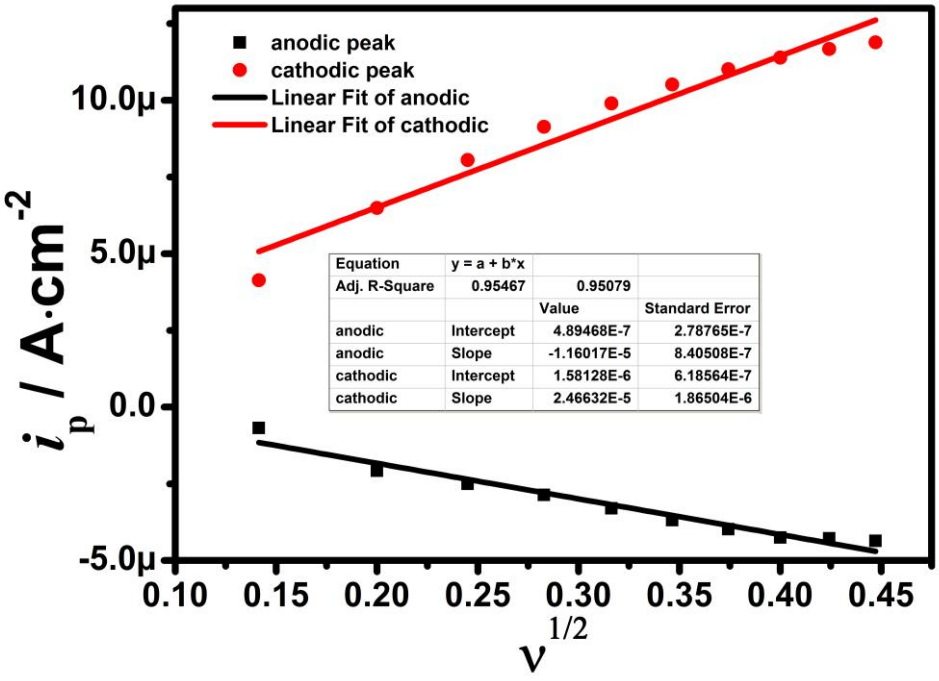

Fig. S7. Plots and parameters of i_{pa} and i_{pc}vs square root of scan rate $\upsilon^{1/2}$ for Fig. 2 (b).

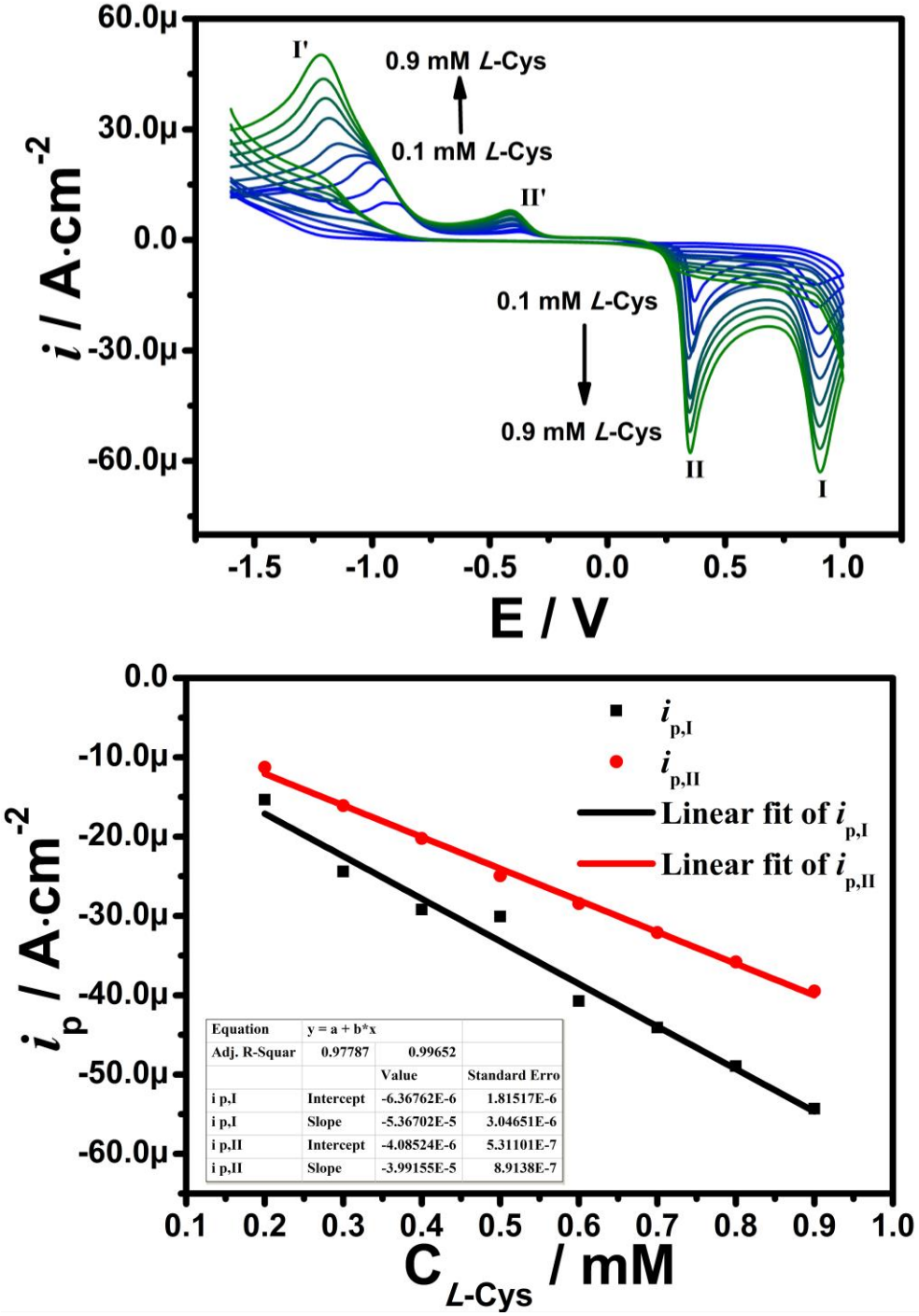

Fig. S8. Top: CVs of **Zn-2/AuE** in DMF-$BMIMBF_4$ solution with *L*-Cys concentrations of 0.1, 0.2, 0.2, 0.4, 0.5, 0.6, 0.7, 0.8, 0.9 mM. Below: Plots of $i_{p,I}$ and $i_{p,II}$ vs *L*-Cys concentration.

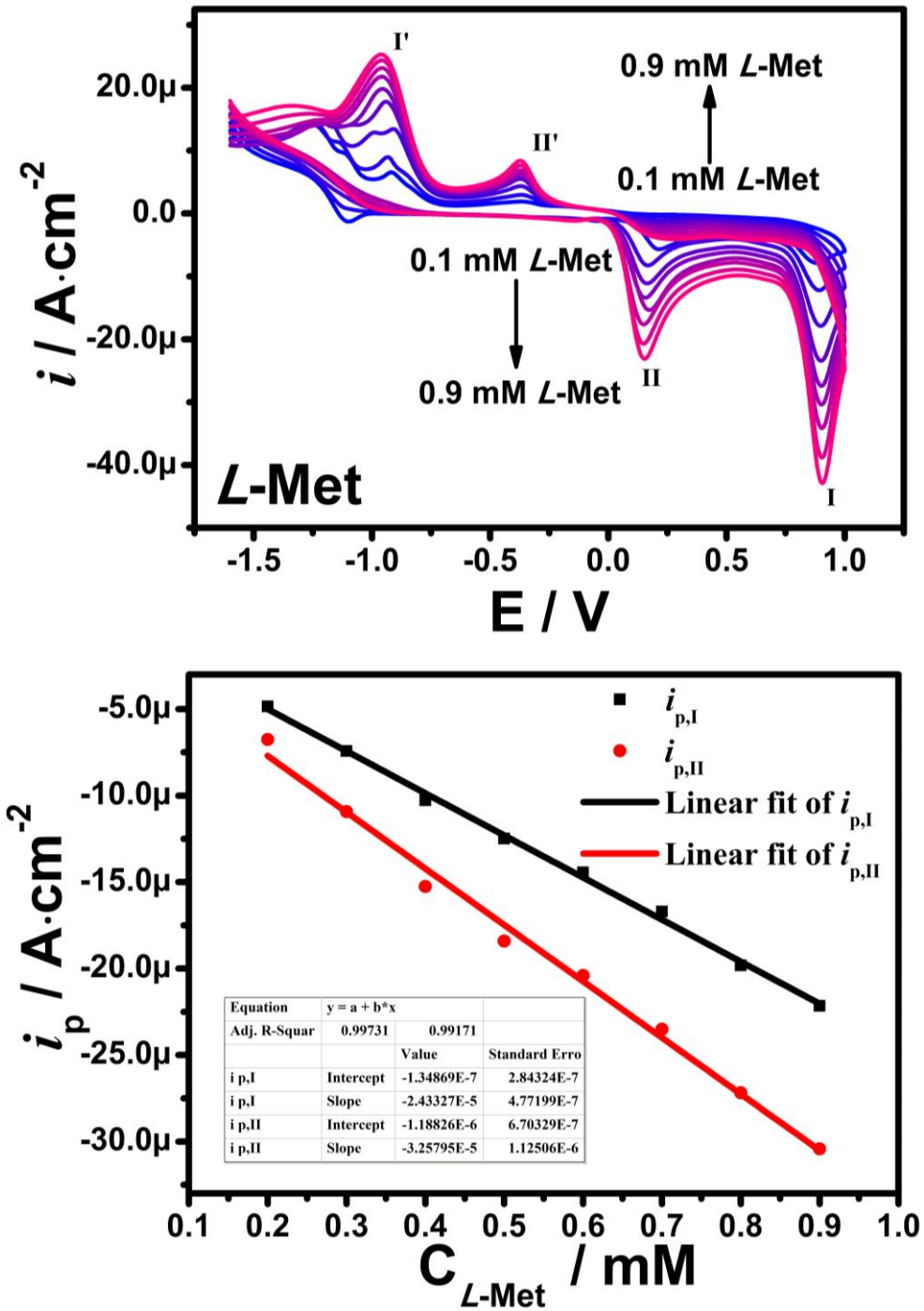

Fig. S9. Top: CVs of **Zn-2/AuE** in DMF-$BMIMBF_4$ solution with *L*-Met concentrations of 0.1, 0.2, 0.2, 0.4, 0.5, 0.6, 0.7, 0.8, 0.9 mM. Below: Plots of $i_{p,I}$ and $i_{p,II}$ vs *L*-Met concentration.

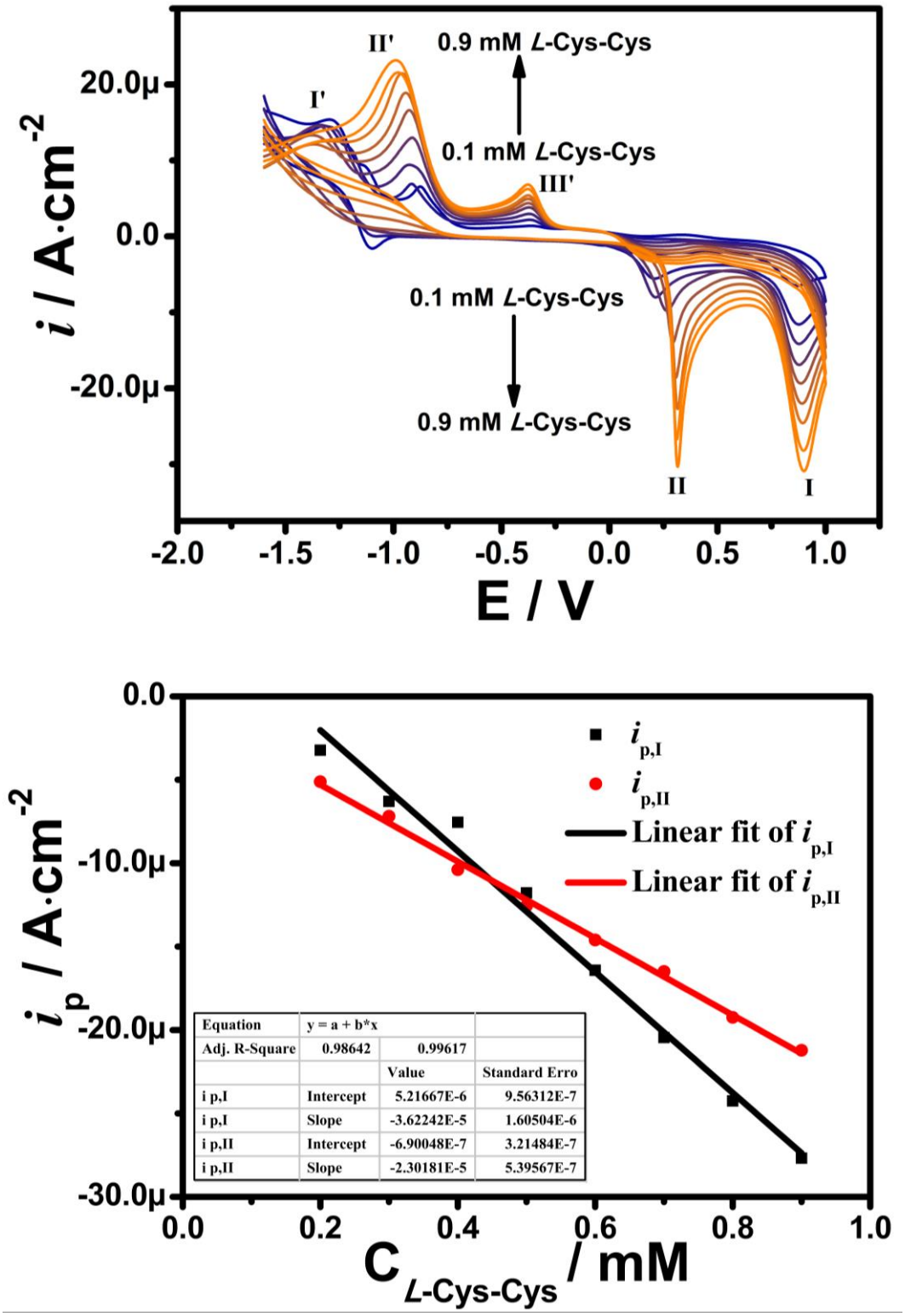

Equation	y = a + b*x		
Adj. R-Square	0.98642	0.99617	
		Value	Standard Erro
i p,I	Intercept	5.21667E-6	9.56312E-7
i p,I	Slope	-3.62242E-5	1.60504E-6
i p,II	Intercept	-6.90048E-7	3.21484E-7
i p,II	Slope	-2.30181E-5	5.39567E-7

Fig. S10. Top: CVs of **Zn-2/AuE** in DMF-$BMIMBF_4$ solution with *L*-Cys-Cys concentrations of 0.1, 0.2, 0.2, 0.4, 0.5, 0.6, 0.7, 0.8, 0.9 mM. Below: Plots of $i_{p,I}$ and $i_{p,II}$ vs *L*-Cys-Cys concentration. In the process of experiment, we added every 10 ul in electrolytic cell, with the increase of concentration, there will be a part of the *L*-Cys-Cys is decomposed into *L*-Cys due to the electrochemical redox effect. It lead to the peak II potential gradully changed from 0.29 V to 0.35 V (*L*-Cys one, Fig. S8(top))

The following points can be seen from the above pictures(Fig. S8and Fig. S10):

(1) For Fig. S10(top): in the process of experiment, we added every 10 ul in electrolytic cell, with the increase of concentration, there will be a part of the *L*-Cys-Cys is decomposed into *L*-Cys due to the electrochemical redox effect. It lead to the peak II potential gradully changed from 0.29 V to 0.35 V (*L*-Cys one, Fig. S8(top)).

(2) what is the cause of *L*-Cys-Cys partial decomposition? First of all, contrasting concentration linear fiting graph of Fig. S10(below) and Fig. S8(below), we can seen that the same concentration of two kinds of different amino acids *L*-Cys-Cys and *L*-Cys, the peak II current density value ($i_{p,II}$)of the gap is very big, for example, 0.5 mM of *L*-Cys $i_{p,II}$ was 3.008 e-5 A, and the same concentration of *L*-Cys-Cys $i_{p,II}$ is only 1.178 e-5 A. Thus, It comfirmed that the *L*-Cys-Cys part decomposition. Secondly, comparing the concentration-peak current density curve (c-$i_{p,II}$) of Fig. S10 (below) and Fig. S8(below), it is obvious that $i_{p,II}$ of *L*-Cys-Cys varies greatly as the increasing of the concentration (the slope value of red line (Fig. S10(below)) -2.30181e-5 A·cm^{-2}> the slope value of red line (Fig. S8(below)) -3.99155e-5 A·cm^{-2}). As the concentration of *L*-Cys-Cys increases, the amount of decomposed *L*-Cys also increases, which increases the change rate of $i_{p,II}$.

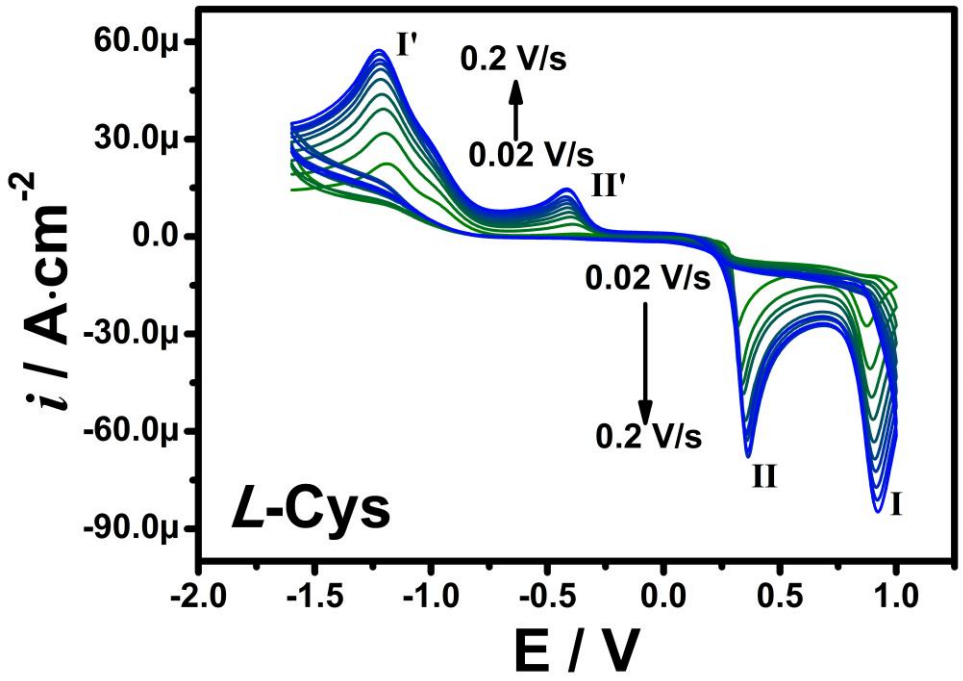

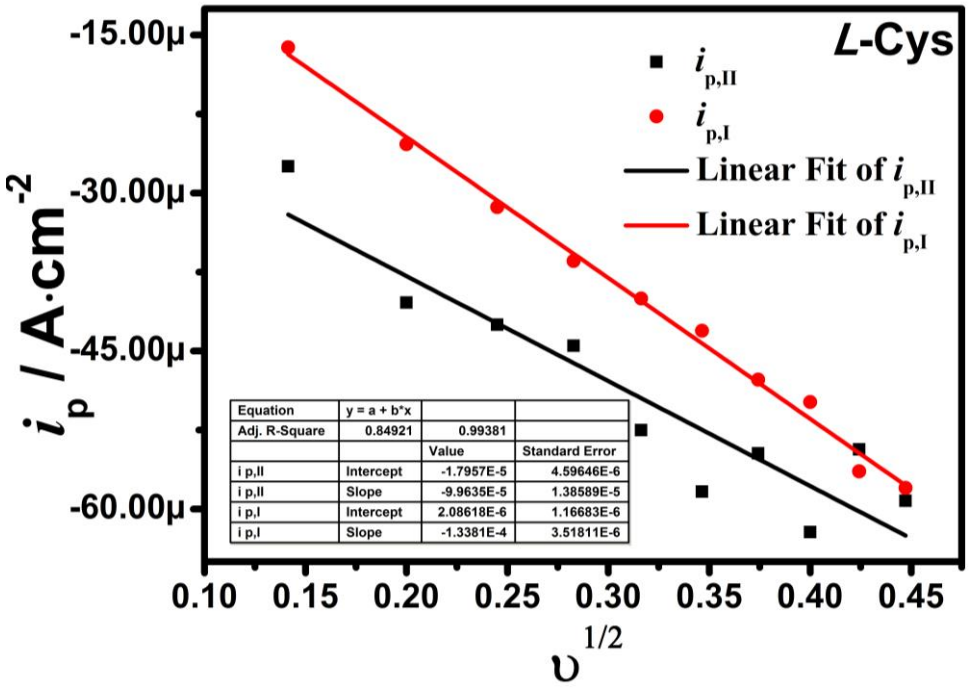

Fig. S11. Top: CVs of **Zn-2/AuE** in DMF-$BMIMBF_4$ solution with 0.9 mM *L*-Cys at different scan rates from 0.02 V·s^{-1} to 0.2 V·s^{-1}. Below: Plots of $i_{p,I}$ and $i_{p,II}$ vs square root of scan rates (υ$^{1/2}$), respectively.

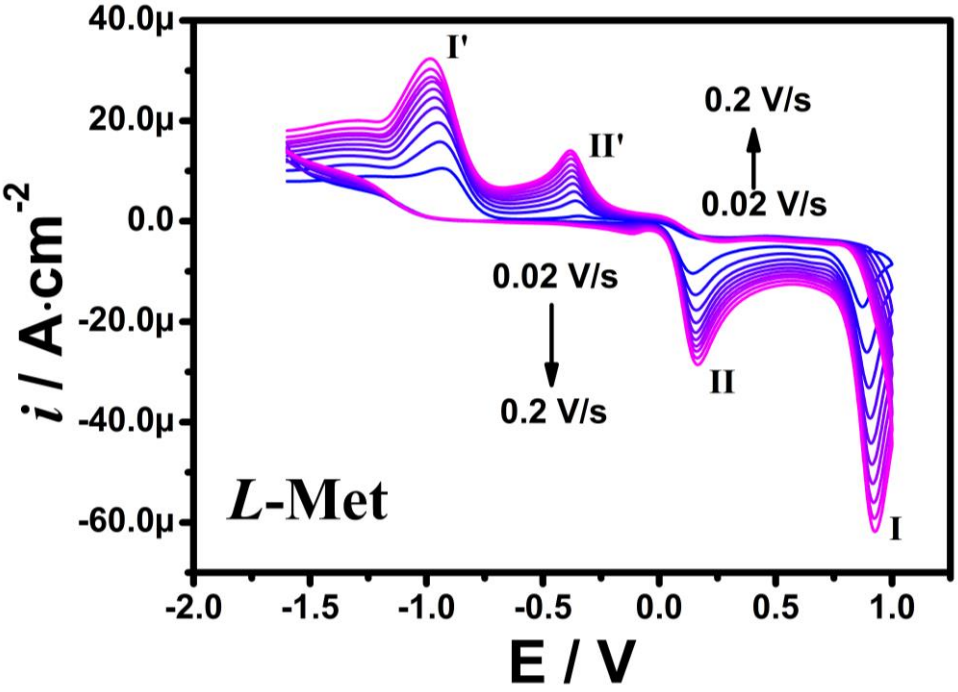

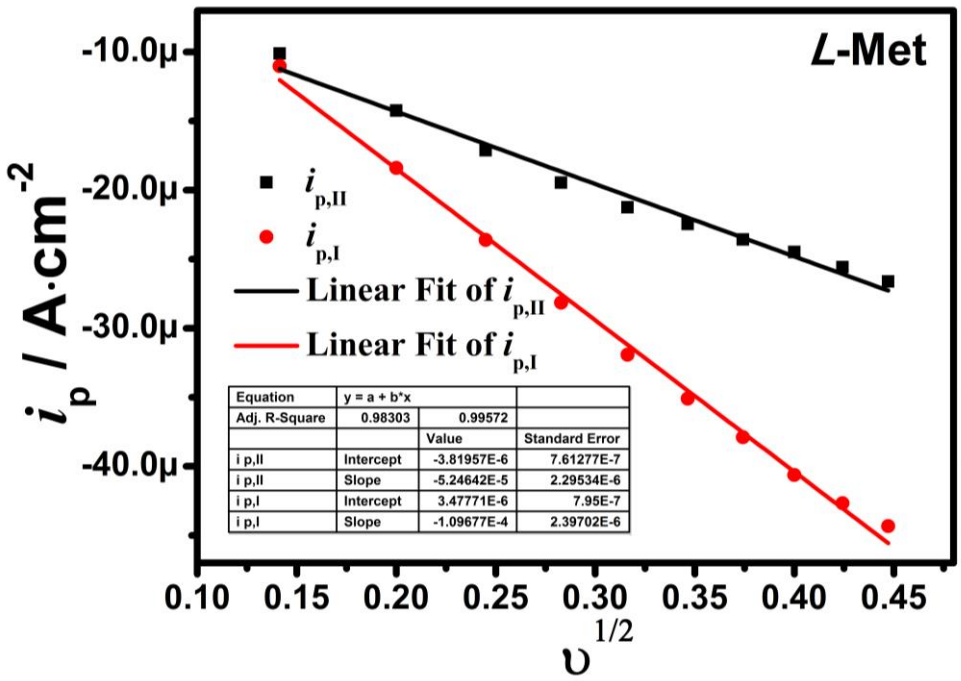

Fig. S12. Top: CVs of **Zn-2/AuE** in DMF-$BMIMBF_4$ solution with 0. 9 mM *L*-Met at different scan rate from 0.02 $V \cdot s^{-1}$ to 0.2 $V \cdot s^{-1}$. Below: Plots of $i_{p,I}$ and $i_{p,II}$ vs $\upsilon^{1/2}$, respectively.

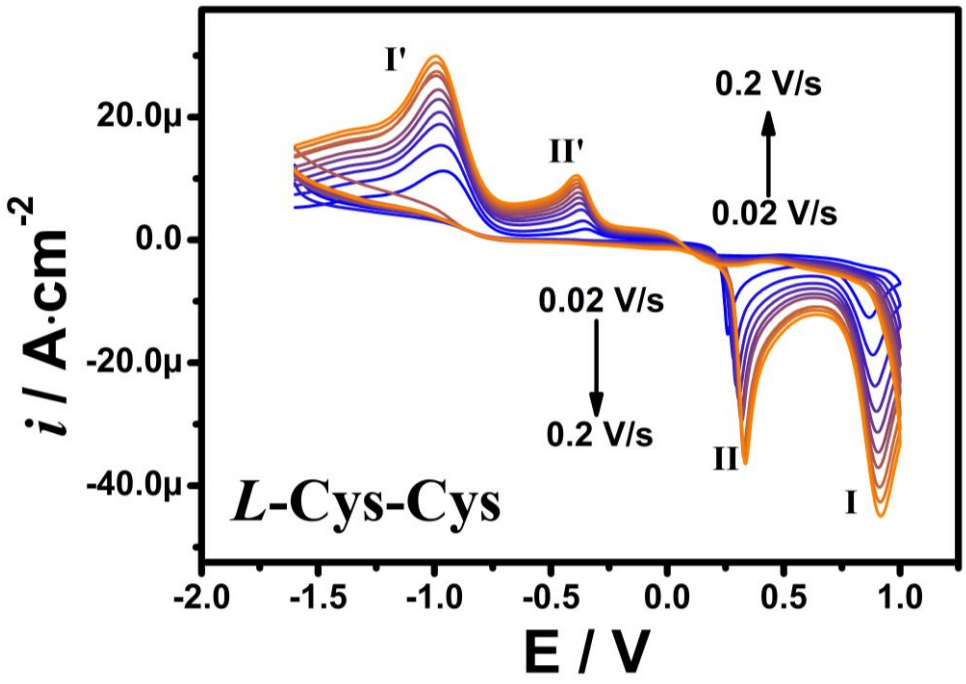

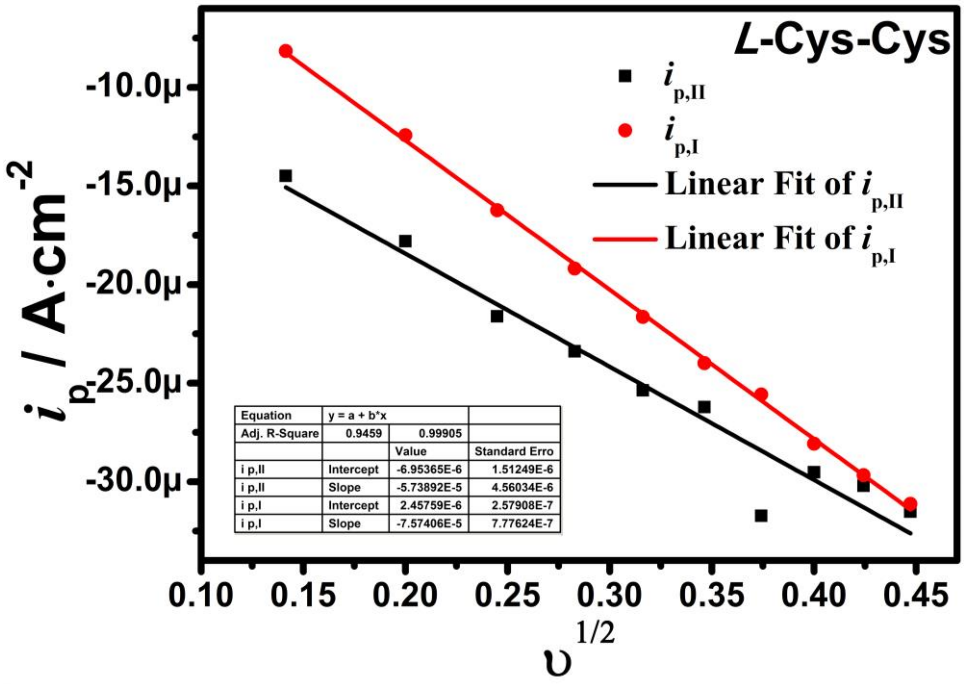

Fig. S13. Top: CVs of **Zn-2/AuE** in DMF-BMIMBF$_4$ solution with 0. 9 mM *L*-Cys-Cys at different scan rate from 0.02 V·s^{-1} to 0.2 V·s^{-1}. Below: Plots of $i_{p,I}$ and $i_{p,II}$ vs $\upsilon^{1/2}$, respectively.